J. Fluid Mech. (1969), *vol.* 38, *part* 4, *pp.* 843–854
Printed in Great Britain

Swirling flow in tubes of non-uniform cross-sections

By CHUEN-YEN CHOW†
Department of Aerospace Engineering Sciences, University of Colorado

(Received 16 May 1969)

A fluid swirling through an axisymmetrically deformed tube is considered, ignoring viscosity and compressibility. For a tube of radius R, having a longitudinal wall deformation of wave number k, the flow near the wall is blocked, if the Rossby number assumes one of the critical values $(\lambda_n^2 + k^2R^2)^{-\frac{1}{2}}$, where n is any positive integer, and λ_n is the nth zero of the Bessel function $J_1(\lambda)$. Rossby number is defined as $W/2R\omega$, in which W and ω are the uniform axial and angular velocities in an undeformed tube. For a convergent-divergent nozzle, the critical Rossby numbers have the same form, with $kR = 0$. The flow exhibits radically different patterns when each critical Rossby number is crossed.

1. The governing equation

This paper deals with a class of steady, axisymmetric, swirling flows of an inviscid, incompressible fluid confined within a tube. Let u, v and w denote respectively the velocity components in the directions of increasing r, θ, and z, the cylindrical co-ordinates fixed in space, where the z-axis coincides with the centre line of the tube. If far upstream from a disturbance the fluid is rotating with constant angular speed ω about the z-axis, and the axial velocity is uniform and equal to W, the governing equation was derived by Long (1953); it has the form,

$$\left(\frac{\partial^2}{\partial r^2} - \frac{1}{r}\frac{\partial}{\partial r} + \frac{\partial^2}{\partial z^2}\right)\psi + \frac{4\omega^2}{W^2}\psi = \frac{2\omega^2}{W}r^2. \tag{1}$$

Here, ψ is the Stokes stream function; the radial and axial velocity components can be obtained from ψ, through the relations,

$$u = -\frac{1}{r}\frac{\partial\psi}{\partial z}, \quad w = \frac{1}{r}\frac{\partial\psi}{\partial r}. \tag{2}$$

As pointed out by Yih (1965, p. 257), since the equation is not obtained by linearization but is exact, the amplitude of the motion need not be small. Many solutions for steady flows of large amplitude were obtained (e.g. those for the pipe flow of a rotating fluid into a sink, by Long 1956 and by Yih, O'Dell & Debler 1962, and those for a like flow past a symmetrically located sphere, by Lai 1964). In the present work, (1) will be solved so as to study the behaviour of a rotating fluid through tubes with axisymmetric deformations along the length.

† Also: Cooperative Institute for Research in Environmental Sciences, University of Colorado.

2. A tube with small sinusoidal deformation along the axis

For simpler analysis let us first consider a swirling flow confined within a tube of radius R, whose wall is deformed into a shape described by

$$r_w = R + a\cos kz, \tag{3}$$

where a is the amplitude and k the wave-number of the sinusoidal deformation. By assuming $(a/R) \ll 1$, the condition that the flow is tangent to the wall becomes approximately

$$\left(\frac{u}{W}\right)_{r=R} = \frac{dr_w}{dz}, \tag{4}$$

and solutions of (1) in simple closed form can readily be obtained. Substituting the assumed stream function

$$\psi = \tfrac{1}{2}Wr^2 + f(r)\cos kz$$

into (1), we have

$$\left[\frac{d^2}{dr^2} - \frac{1}{r}\frac{d}{dr} - \frac{1}{R^2}(k^2R^2 - R_0^{-2})\right] f = 0, \tag{5}$$

where $R_0 = W/2R\omega$ is the Rossby number. Equation (5) gives three possible solutions, depending upon the magnitude of $(k^2R^2 - R_0^{-2})$. Satisfying the boundary condition (4), the corresponding stream functions and axial velocities are, for $R_0^{-2} < k^2R^2$,

$$\frac{\psi}{\frac{1}{2}WR^2} = \left(\frac{r}{R}\right)^2 - 2\frac{ar}{R^2}\frac{I_1\{\sqrt{(k^2R^2 - R_0^{-2})}\, r/R\}}{I_1\{\sqrt{(k^2R^2 - R_0^{-2})}\}}\cos kz, \tag{6}$$

$$\frac{w}{W} = 1 - \frac{a}{R}(k^2R^2 - R_0^{-2})^{\frac{1}{2}}\frac{I_0\{\sqrt{(k^2R^2 - R_0^{-2})}\, r/R\}}{I_1\{\sqrt{(k^2R^2 - R_0^{-2})}\}}\cos kz, \tag{7}$$

for $R_0^{-2} = k^2R^2$,

$$\frac{\psi}{\frac{1}{2}WR^2} = \left(\frac{r}{R}\right)^2\left(1 - 2\frac{a}{R}\cos kz\right), \tag{8}$$

$$\frac{w}{W} = 1 - 2\frac{a}{R}\cos kz, \tag{9}$$

and, finally, for $R_0^{-2} > k^2R^2$,

$$\frac{\psi}{\frac{1}{2}WR^2} = \left(\frac{r}{R}\right)^2 - 2\frac{ar}{R^2}\frac{J_1\{\sqrt{(R_0^{-2} - k^2R^2)}\, r/R\}}{J_1\{\sqrt{(R_0^{-2} - k^2R^2)}\}}\cos kz, \tag{10}$$

$$\frac{w}{W} = 1 - \frac{a}{R}(R_0^{-2} - k^2R^2)^{\frac{1}{2}}\frac{J_0\{\sqrt{(R_0^{-2} - k^2R^2)}\, r/R\}}{J_1\{\sqrt{(R_0^{-2} - k^2R^2)}\}}\cos kz. \tag{11}$$

The effect of rotation on axial velocity at the throat, $kz = \pi$, is shown in figure 1 plotted for $kR = 3$ and $a/R = 0{\cdot}1$. Without rotation, $R_0^{-1} = 0$, the velocity on the axis is lower than that at the wall. Increasing ω accelerates the central flow, and decelerates the flow near the boundary. When $R_0^{-1} = kR$, the axial velocity becomes uniform across any section as indicated by (9). The effect of increasing ω remains the same until $(R_0^{-2} - k^2R^2)^{\frac{1}{2}}$ reaches the value $\lambda_1 (= 3{\cdot}83171)$; λ_n designates the nth zero of the function $J_1(\lambda)$. It should be noted that, when

$(R_0^{-2} - k^2R^2)^{\frac{1}{2}}$ is in the neighbourhood of λ_n, equation (11) shows that w at the wall deviates largely from W and therefore the approximated condition (4) cannot be used. In this case, the results (6)–(11) become invalid.

When the parameter $(R_0^{-2} - k^2R^2)^{\frac{1}{2}}$ exceeds λ_1, the effect of increasing ω becomes different. At the throat, the flow decelerates at the centre, accelerates in an outer region, and then decelerates again near the wall. This is illustrated in figure 2 by the curves $R_0^{-2} = 34$ and 45, plotted for the same kR, but a much

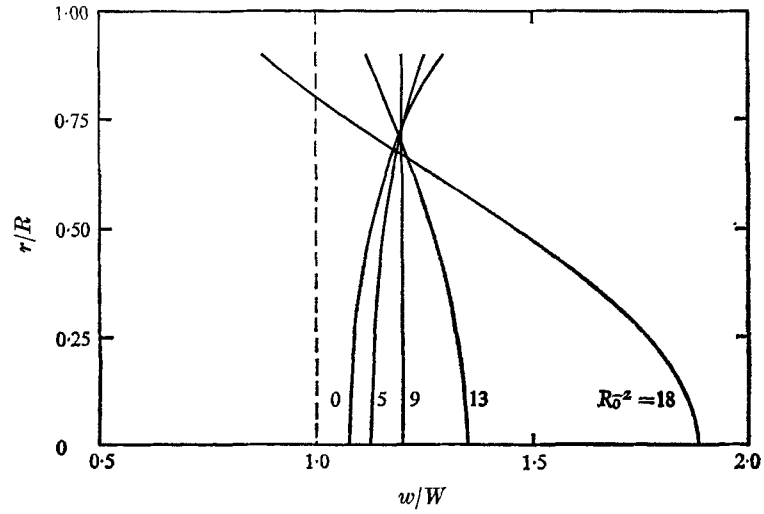

FIGURE 1. At low angular speeds, the effect of increasing angular speed on the axial velocity across the throat of a sinusoidally deformed tube with $kR = 3$ and $a/R = 0{\cdot}1$.

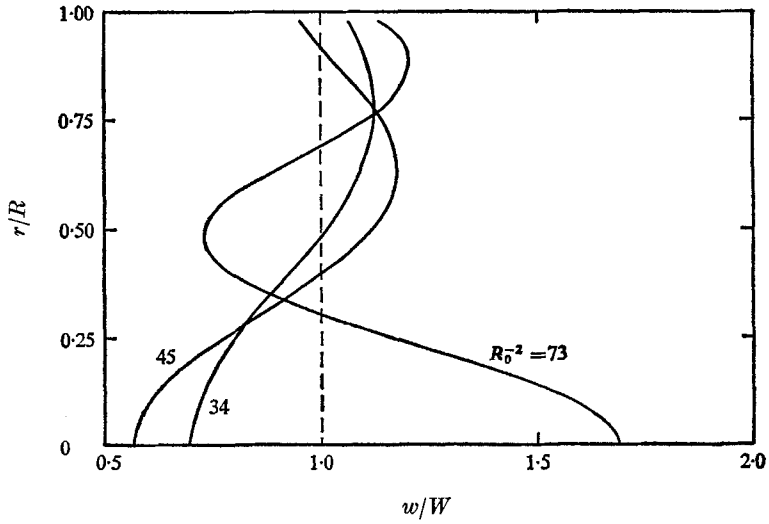

FIGURE 2. At higher angular speeds, the effect of increasing angular speed on the axial velocity across the throat of a sinusoidally deformed tube with $kR = 3$ and $a/R = 0{\cdot}02$.

smaller amplitude, $a/R = 0{\cdot}02$. When that parameter becomes greater than $\lambda_2(= 7{\cdot}01559)$, another radical change occurs. The curve $R_0^{-2} = 73$ shows that the central fluid at the throat is accelerated again.

With further increase in angular speed, the effect on the central axial velocity reverses each time $(R_0^{-2} - k^2R^2)^{\frac{1}{2}}$ exceeds λ_3, λ_4, etc., and large velocity changes can be caused by a small wall deformation as revealed by (11).

Thus, we have found that there exist infinitely many critical Rossby numbers of the values,

$$(R_0)_{\mathrm{cr}} = (\lambda_n^2 + k^2R^2)^{-\frac{1}{2}} \quad (n = 1, 2, 3, \ldots). \tag{12}$$

At these critical angular speeds, no solution of (1) can be found to satisfy the boundary condition (4). Physically speaking, the fluid cannot go around the humps at the wall, and is expected to become stagnant in that region. This is the phenomenon of blocking, which occurs in a rotating and in a stratified fluid flow, discussed in detail by Yih (1965). The flow patterns with blocking will be obtained in § 4 which concerns a convergent-divergent nozzle.

The angular velocity is expressed by

$$v = \frac{2\omega}{W}\frac{\psi}{r}, \tag{13}$$

obtained from the condition that angular momentum of a fluid particle is conserved along its streamline. It shows that the angular velocity increases or decreases when a particle is deflected towards or away from the tube axis.

3. Tubes with large periodic wall deformations

If one does not specify the shape of wall deformation *a priori*, as we did in § 2, exact solutions can be obtained for a rotating flow through tubes with large-amplitude deformations by using an inverse method, which may show reversed flows in the fluid. For example, if $|R_0^{-1}| > kR$,

$$\frac{\psi}{\frac{1}{2}WR^2} = \left(\frac{r}{R}\right)^2 + C\frac{r}{R}J_1\left\{\sqrt{(R_0^{-} - k^2R^2)}\frac{r}{R}\right\}\cos kz \tag{14}$$

is an exact solution of (1). It represents flows bounded by a wall described by the equation $\psi/\frac{1}{2}WR^2 = 1$, whose shape is controlled by the arbitrary constant C, which is not necessarily small. Some of the flow patterns, and the corresponding axial velocity distributions, are plotted for $kR = 2$ and for values of C, determined in such a way that the radius at the throat is $0{\cdot}9R$. Because of symmetry, only the section $\pi \leqslant kz \leqslant 2\pi$ is shown.

Figure 3, based on $R_0^{-1} = 4$, shows that the velocity across the throat is at a maximum in the centre. This central flow decelerates continuously downstream, and the flow becomes separated from the axis, to form a reversed flow in the region of larger cross-sections. Figure 4 is plotted for a higher angular speed, $R_0^{-1} = 6$. Now $(R_0^{-2} - k^2R^2)^{\frac{1}{2}}$ is greater than λ_1 but, less than λ_2, and this flow behaves entirely differently from the previous one. The reverse-flow region moves into the throat, and the central velocity becomes highest at the section where the area is at a maximum. At a still higher angular speed corresponding to $R_0^{-1} = 9$,

which is in the region $\lambda_2 < (R_0^{-2} - k^2R^2)^{\frac{1}{2}} < \lambda_3$, figure 5 shows that the central separated region moves back from the throat to the section of maximum area. Wrapping around this cylindrical core of separation, there appears an annular ring of backflow close to the wall. The annular-ring flow pattern also appears within the throat.

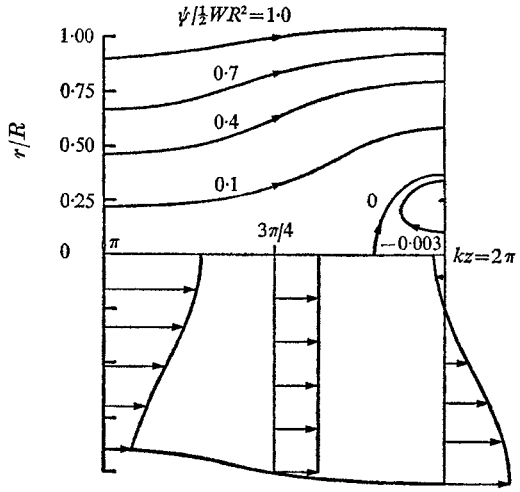

FIGURE 3. Streamlines and axial velocity profiles in a rotating flow at $R_0^{-1} = 4$ through a wavy tube with $kR = 2$ and $C = 0{\cdot}718$.

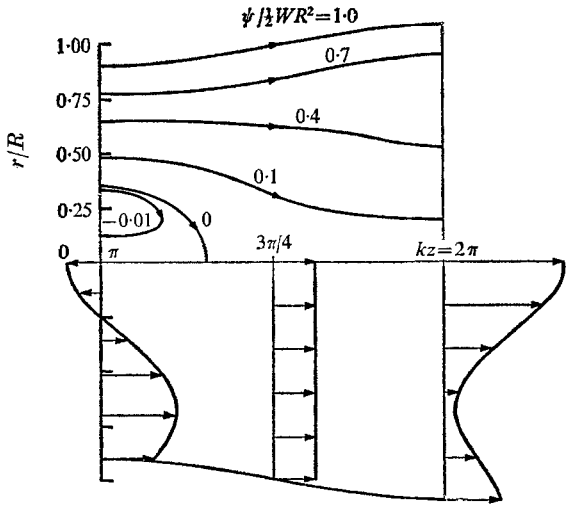

FIGURE 4. Streamlines and axial velocity profiles in a rotating flow at $R_0^{-1} = 6$ through a wavy tube with $kR = 2$ and $C = -0{\cdot}628$.

The general flow behaviour at various angular speeds is similar to that discussed in § 2 except the velocity changes are magnified. More complicated flow patterns can be obtained if the Rossby number is reduced further.

It is interesting to compare the theoretical result with the experimental work reported by Gore & Ranz (1964). They dealt with a swirling air flow expanding freely from the opening of a uniform tube into the atmosphere, instead of that moving through an alternatively convergent-divergent nozzle. However, the similarities between the two for the flow near the throat are striking. Let the Rossby number of their flow be computed, based on the tube radius and on the assumed axial velocity in the tube. In the experiment of Gore & Ranz at $R_0^{-1} = 3{\cdot}14$, a well-defined backflow appeared outside the tube, where the flow was divergent; this looked very similar to the pattern in figure 3. At $R_0^{-1} = 8{\cdot}6$, Gore & Ranz found that part of the separated flow moved into the opening of the tube; this is analogous to the flow in figure 4. Had the experiment run at higher swirl ratios, the annular rings of separation plotted in figure 5 might have been observed. Gore & Ranz also observed critical swirl ratios. Because of different geometric configurations, their critical Rossby numbers do not correspond to those obtained in (12).

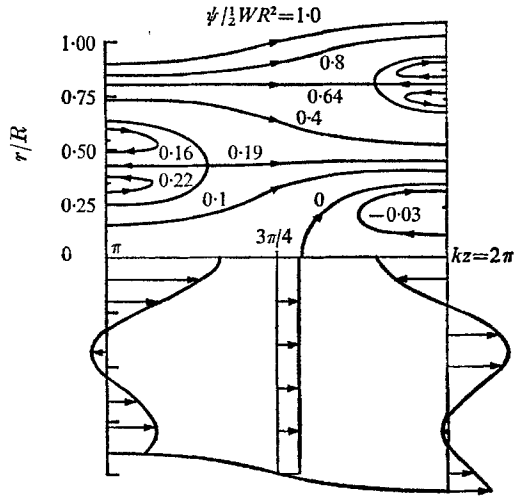

FIGURE 5. Streamlines and axial velocity profiles in a rotating flow at $R_0^{-1} = 9$ through a wavy tube with $kR = 2$ and $C = 0{\cdot}965$.

When critical Rossby numbers are reached, (14) describes all the possible internal waves inside a straight tube (which will be discussed in the next section).

4. Convergent-divergent nozzles

We are now concerned with a swirling flow moving through a convergent-divergent nozzle. The inverse method of Fraenkel (1956) is adopted, in which the wall shape is not specified *a priori*. Let R be the radius of the undeformed tube. From the fact that far upstream the longitudinal velocity is W and the fluid is rotating with constant angular speed ω, the general solution of (1) can

be written separately for the upstream and downstream regions. One gets, respectively,

$$\psi_- = WR^2\left[\frac{1}{2}\left(\frac{r}{R}\right)^2 + \sum_{N+1}^{\infty} a_n e^{p_n z}\frac{r}{R}J_1\left(\lambda_n\frac{r}{R}\right)\right], \quad \text{for} \quad z \leqslant 0, \tag{15}$$

$$\psi_+ = WR^2\left[\frac{1}{2}\left(\frac{r}{R}\right)^2 + \sum_{n=1}^{N}(b_n \sin k_n z + c_n \cos k_n z)\frac{r}{R}J_1\left(\lambda_n\frac{r}{R}\right) + \sum_{N+1}^{\infty} d_n e^{-p_n z}\frac{r}{R}J_1\left(\lambda_n\frac{r}{R}\right)\right], \quad \text{for} \quad z \geqslant 0, \tag{16}$$

in which

$$p_n R = (\lambda_n^2 - R_0^{-2})^{\frac{1}{2}}, \tag{17}$$

$$k_n R = (R_0^{-2} - \lambda_n^2)^{\frac{1}{2}}, \tag{18}$$

and the integer N is defined by the relation

$$\lambda_N < |R_0^{-1}| \leqslant \lambda_{N+1}. \tag{19}$$

Rossby number and λ_n are the same as those defined previously in § 2. In the case $N = 0$, all the terms containing trigonometric functions in (16) are dropped.

The coefficients a_n, b_n, c_n and d_n are to be determined from the requirements that

$$\psi_- = \psi_+ \quad \text{at} \quad z = 0, \tag{20}$$

$$\frac{\partial \psi_-}{\partial z} - \frac{\partial \psi_+}{\partial z} = f(r) \quad \text{at} \quad z = 0, \tag{21}$$

in which $f(r) = 0$ for $0 \leqslant r < r_1$. $f(r)$ represents a distribution of ring vortices of variable strength at $z = 0$, extending over the range $r_1 \leqslant r \leqslant R$, which implicitly determines the shape of the barrier at the wall. Instead of a vortex sheet, Fraenkel used source and sink distributions to generate desired body shapes.

The condition (20) requires that

$$a_n = d_n \quad \text{for} \quad n > N \quad \text{and} \quad c_n = 0 \quad \text{for} \quad n \leqslant N. \tag{22}$$

Equations (15), (16) and (22) reduce (21) to:

$$2\sum_{N+1}^{\infty} a_n p_n \frac{r}{R}J_1\left(\lambda_n\frac{r}{R}\right) - \sum_{n=1}^{N} b_n k_n \frac{r}{R}J_1\left(\lambda_n\frac{r}{R}\right) = f(r). \tag{23}$$

For simpler computations let us choose the function,

$$f(r) = Q\frac{r}{R}J_1\left(\lambda_1\frac{r}{R}\right), \quad \text{for} \quad r_1 \leqslant r \leqslant R, \tag{24}$$

where Q is an arbitrary constant. Multiplying (23) by $J_1\{\lambda_m(r/R)\}dr$, and integrating between the limits $r = 0$ and R, we obtain the following by using orthogonality relationships. For $n = 1$,

$$a_1 = \frac{Q}{2p_1 R J_0^2(\lambda_1)}\left\{J_0^2(\lambda_1) - \left(\frac{r_1}{R}\right)^2\left[J_0^2(\chi_1) + J_1^2(\chi_1) - \frac{2}{\chi_1}J_0(\chi_1)J_1(\chi_1)\right]\right\}, \tag{25}$$

$$b_1 = -\frac{Q}{k_1 R J_0^2(\lambda_1)}\left\{J_0^2(\lambda_1) - \left(\frac{r_1}{R}\right)^2\left[J_0^2(\chi_1) + J_1^2(\chi_1) - \frac{2}{\chi_1}J_0(\chi_1)J_1(\chi_1)\right]\right\}, \tag{26}$$

and, for $n > 1$,

$$a_n = \frac{Qr_1/R}{p_n R(\lambda_n^2 - \lambda_1^2) J_0^2(\lambda_n)} [\lambda_n J_0(\chi_n) J_1(\chi_1) - \lambda_1 J_0(\chi_1) J_1(\chi_n)], \tag{27}$$

$$b_n = -\frac{2Qr_1/R}{k_n R(\lambda_n^2 - \lambda_1^2) J_0^2(\lambda_n)} [\lambda_n J_0(\chi_n) J_1(\chi_1) - \lambda_1 J_0(\chi_1) J_1(\chi_n)], \tag{28}$$

in which $\chi_m = \lambda_m r_1/R$.

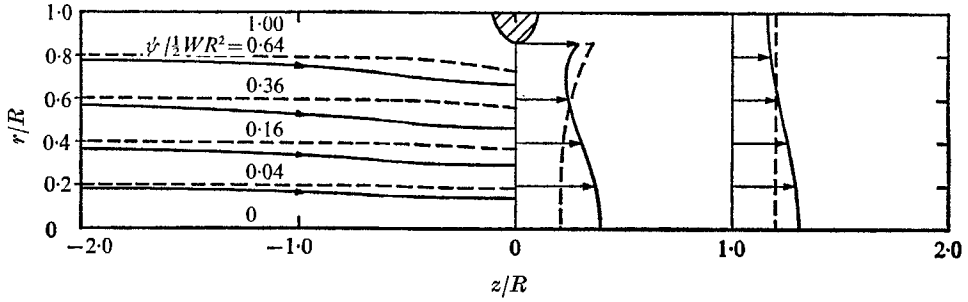

FIGURE 6. Streamlines and axial velocity profiles in a rotating flow at $R_0^{-1} = 3{\cdot}73$ through a nozzle based on $r_1 = 0{\cdot}9$ and $Q = 118{\cdot}11$. Dashed lines in this and some of the following figures represent those in a non-rotating flow at $R_0^{-1} = 0$, based on $r_1 = 0{\cdot}9$ and $Q = 204{\cdot}35$.

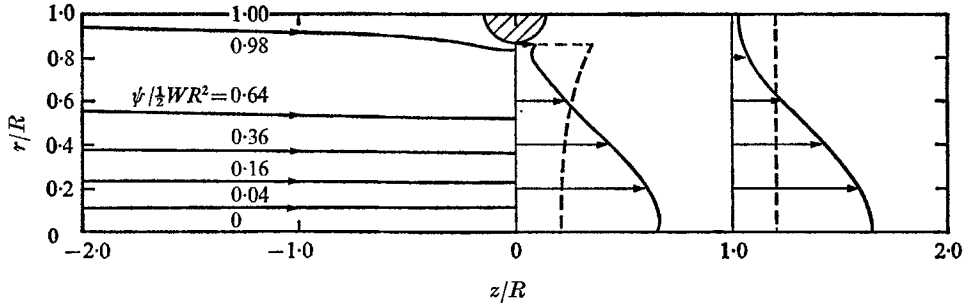

FIGURE 7. A rotating flow at $R_0^{-1} = 3{\cdot}831$ through a nozzle based on $r_1 = 0{\cdot}9$ and $Q = 19{\cdot}26$.

By assigning different values to r_1 and Q, one can obtain various contours for the nozzle described by the equations $\psi \pm = \frac{1}{2}WR^2$. It is tedious to adjust their values so that the nozzle shape becomes the same for different flows. To simplify our work, the value of r_1 is fixed at $0{\cdot}9\,R$, and Q is so chosen that the radius of the throat is always $0{\cdot}86R$. The zeros of J_1 used in our calculations are those up to λ_{12}. It has been found that the barriers so generated do not vary too much in shape if the Rossby number is not too close to $1/\lambda_n$, where n denotes any positive integer. Flows of the same flow rate, but at increasing angular speed, moving through nozzles of the same contraction ratio, are presented in figures 6–15.

When $|R_0^{-1}|$ is less than λ_1, or $N = 0$, equation (16) indicates that downstream

waves do not appear and the flow is symmetric about $z = 0$. A representative flow at $R_0^{-1} = 3{\cdot}73$ is plotted in figure 6 in comparison with the non-rotating flow at $R_0^{-1} = 0$. The shapes of the nozzle for these two flows are almost identical. When going through a contraction, the streamlines of the rotating fluid deflect more towards the axis, as shown on the left half of the figure. Axial velocity profiles at $z = 0$ and R are plotted on the right, showing the deceleration of the central region after the throat. At $R_0^{-1} = 3{\cdot}831$, which is a little less than λ_1, a wider barrier is produced in figure 7. The flow concentrates more towards the axis, and the wall contraction has a far-reaching influence in the fluid. The axial flow near the wall becomes almost stagnant both up- and downstream from the barrier.

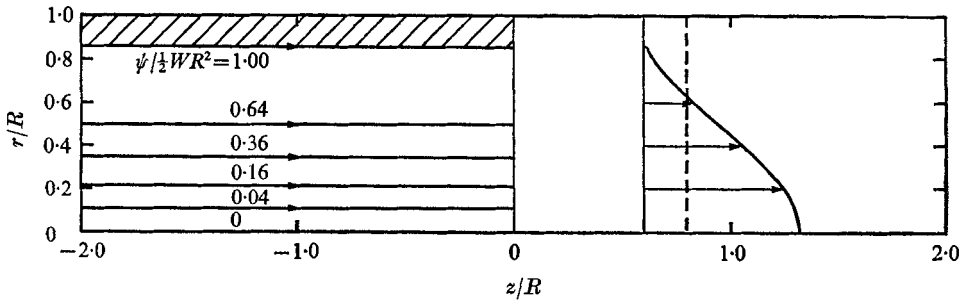

FIGURE 8. First blocking at $R_0^{-1} = 3{\cdot}83171$ or λ_1.

When the value of R_0^{-1} increases more towards λ_1, the coefficient a_1 increases very rapidly as can be seen in (25), and the barrier becomes further elongated. At the limit, when $R_0^{-1} = \lambda_1$, the expression (25) can no longer be used, and (15) and (16) take the form

$$\psi_{\mp} = WR^2\left[\frac{1}{2}\left(\frac{r}{R}\right)^2 + a_1\frac{r}{R}J_1\left(\lambda_1\frac{r}{R}\right)\right]; \tag{29}$$

the flow is now independent of z. The requirement, that the outmost streamline $\psi = \frac{1}{2}WR^2$ contracts to a throat of radius $0{\cdot}86R$, determines the value of a_1. Figure 8 shows that the barrier becomes a straight cylindrical surface. In other words, under this critical condition, if a barrier is placed at $z = 0$, the flow up- and downstream from the body is completely blocked, and the tube cross-section is effectively reduced. When this happens, the uniform upstream conditions cannot be assumed.

Immediately after this critical value is passed, (16) indicates that a wave of the form $\sin k_1 z$ appears downstream from the throat, and the flow pattern becomes non-symmetric and basically different. Such a flow at $R_0^{-1} = 3{\cdot}832$ is plotted in figure 9, which shows that a large cylinder of reversed flow occupies most of the tube downstream from the throat, and that the main flow is accelerated toward the tube boundary. The separated flow rejoins the axis at a large distance $z = \pi/k_1$, approximately, and then separates again at approximately $z = 2\pi/k_1$. A similar pattern will recur thereafter, when the exponential terms are damped out at such a large distance.

Figure 10 shows that at a higher angular speed corresponding to $R_0^{-1} = 5$, the separated regions shrink in size and the distances in between become shorter. It is found at $R_0^{-1} = 6$ that the first reverse bubble moves into the throat, and the downstream bubbles disappear, although a wave pattern is still preserved. Increasing the rotation further, at $R_0^{-1} = 7$ the reversed flow expands again, and the flow becomes nearly symmetric about the throat. The streamlines are plotted in figure 11. The flow behaviour with increasing angular speed observed by Gore & Ranz (1964) again agrees qualitatively with our result.

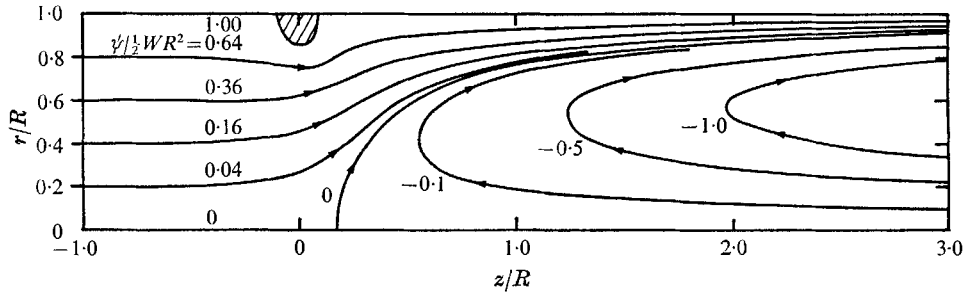

FIGURE 9. A rotating flow at $R_0^{-1} = 3{\cdot}832$ through a nozzle based on $r_1 = 0{\cdot}9$ and $Q = 223{\cdot}60$.

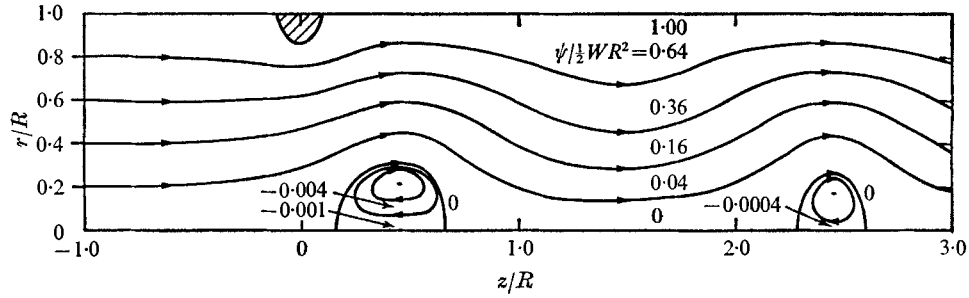

FIGURE 10. A rotating flow at $R_0^{-1} = 5$ through a nozzle based on $r_1 = 0{\cdot}9$ and $Q = 200{\cdot}68$.

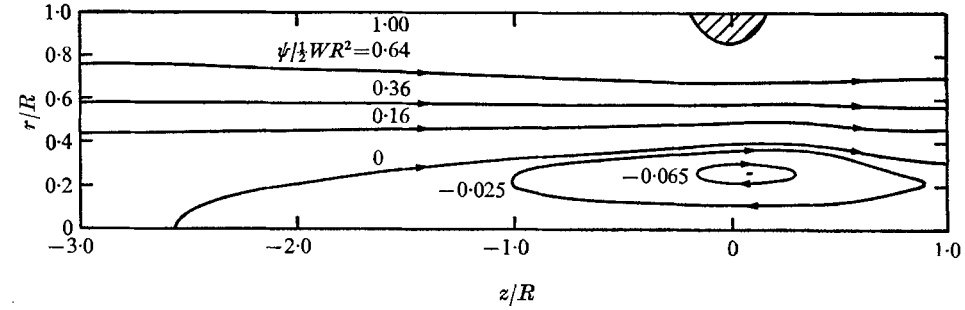

FIGURE 11. A rotating flow at $R_0^{-1} = 7$ through a nozzle based on $r_1 = 0{\cdot}9$ and $Q = 39{\cdot}93$.

When R_0^{-1} approaches λ_2, both the barrier and the separated region are elongated. They extend to infinity when the exact value of λ_2 is reached. The second blocking phenomenon is shown in figure 12. The expression for the stream function is the same as (29), if a_1 and λ_1 are replaced by a_2 and λ_2. Under this second critical condition, the barrier not only blocks the flow near the wall, but also reverses the flow in the central portion. Again the uniform upstream conditions are violated.

Blocking breaks down if R_0^{-1} increases slightly from λ_2 as illustrated in figure 13. At the value 7·016 the flow divides itself into two branches: one accelerates towards the axis, and the other towards the wall. In between, there is an annular

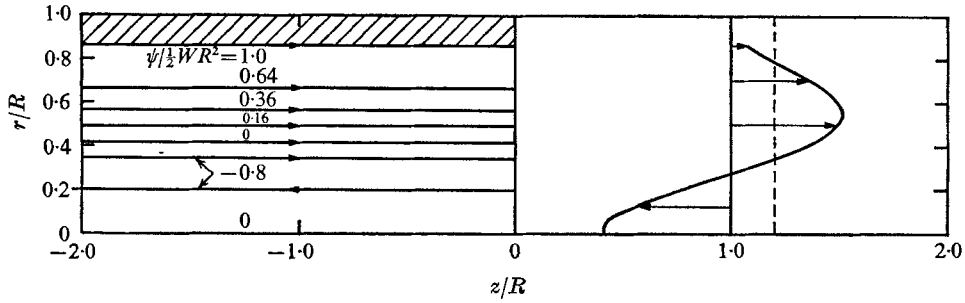

FIGURE 12. Second blocking at $R_0^{-1} = 7{\cdot}01559$ or λ_2.

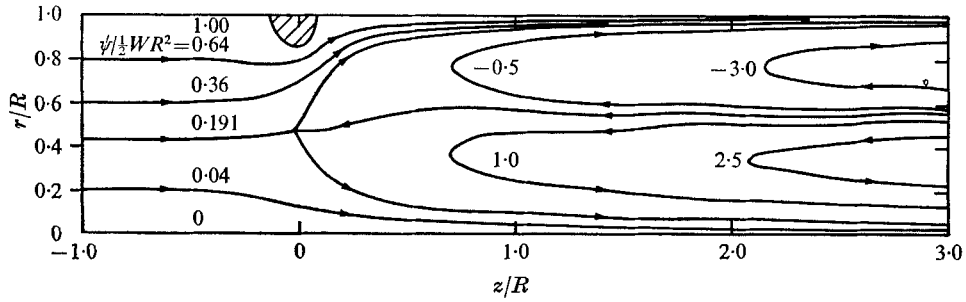

FIGURE 13. A rotating flow at $R_0^{-1} = 7{\cdot}016$ through a nozzle based on $r_1 = 0{\cdot}9$ and $Q = 285{\cdot}80$.

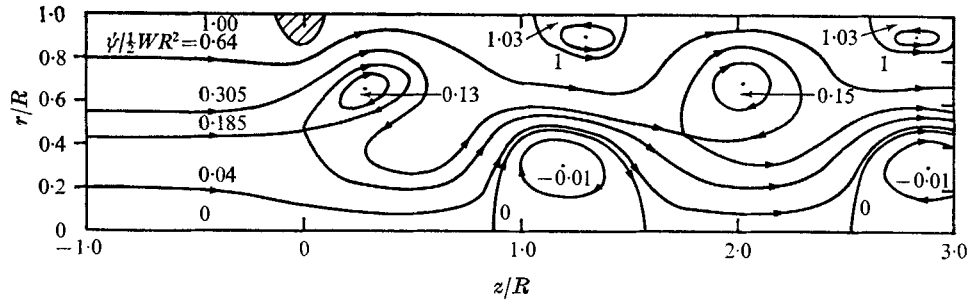

FIGURE 14. A rotating flow at $R_0^{-1} = 8$ through a nozzle based on $r_1 = 0{\cdot}9$ and $Q = 248{\cdot}54$.

reversed region containing a pair of ring vortices, which closes far downstream. Increasing R_0^{-1} to 8, figure 14 shows separations at the axis and the wall appearing in addition to those in the intermediate regions.

The third blocking occurs at $R_0^{-1} = \lambda_3$ (= 10·17347). After that, the flow exhibits a more complicated pattern (represented by figure 15, where it is plotted for $R_0^{-1} = 11$).

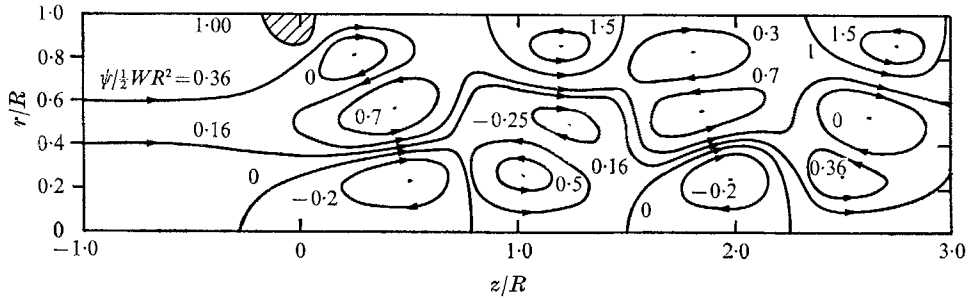

FIGURE 15. A rotating flow at $R_0^{-1} = 11$ through a nozzle based on $r_1 = 0{\cdot}9$ and $Q = 426{\cdot}66$.

In the case of a convergent–divergent nozzle, the critical Rossby numbers for blocking still have the same form as (12) with $kR = 0$, corresponding to a sinusoidally deformed tube with infinitely long wavelength. The flow pattern changes abruptly when the rotational speed of the fluid exceeds each of the critical values.

The problem of a rotating fluid through a convergent–divergent nozzle was tackled by Fraenkel (1956), but in his work only one case in which $R_0^{-1} < \lambda_1$ was discussed. The phenomena of cylindrical core and annular ring of reversed flows were observed in the experiments of Binnie (1957), in which the far flow might not be in a rigid body rotation, and a modified analysis is required.

In contrast with the explanation of Nissan & Bresan (1961), that secondary flows in a rotating fluid are associated with a viscous effect, it has been demonstrated here that such flows are possible in an inviscid swirling flow.

This work was supported in part by the Advanced Research Projects Agency, contract DA 31-124-ARO-D-139, and the Office of Naval Research, contract 1147(10).

REFERENCES

BINNIE, A. M. 1957 *Quart. J. Mech. Appl. Math.* **10**, 276.

FRAENKEL, L. E. 1956 *Proc. Roy. Soc.* A **233**, 506.

GORE, R. W. & RANZ, W. E. 1964 *A.I.Ch.E. Journal* **10**, 83.

LAI, W. 1964 *J. Fluid Mech.* **18**, 587.

LONG, R. R. 1953 *J. Meteor.* **10**, 197.

LONG, R. R. 1956 *Quart. J. Mech. Appl. Math.* **9**, 385,

NISSAN, A. H. & BRESAN, V. P. 1961 *A.I.Ch.E. Journal* **7**, 543.

YIH, C.-S., O'DELL, W. & DEBLER, W. R. 1962 *Proc. 4th U.S. Nat. Congr. Appl. Mech.* 1441.

YIH, C.-S. 1965 *Dynamics of Nonhomogeneous Fluids.* New York: MacMillan.